Structural Analysis of the SiO_2/Si(100) Interface by Means of Photoelectron Diffraction

S. Dreiner,[1,2] M. Schürmann,[1] and C. Westphal[1]

[1]*Universität Dortmund, Lehrstuhl für Experimentelle Physik I, Otto-Hahn-Str. 4, 44221 Dortmund, Germany*
[2]*Westfälische Wilhelms-Universität Münster, Physikalisches Institut, Wilhelm-Klemm-Str. 10, 48149 Münster, Germany*
(Received 20 April 2004; published 16 September 2004)

The local environment of Si atoms at the interface between a thermally grown SiO_2 film and Si(100) was studied by angle-scanned photoelectron diffraction. Experimental photoelectron diffraction patterns for each Si oxidation state were obtained from the results of least squares fitting on Si $2p$ core-level spectra. A comparison of the diffraction patterns with multiple-scattering calculations including an R-factor analysis was performed. An excellent agreement between experimental and simulated data was achieved within the proposed bridge-bonded interface model [Yuhai Tu and J. Tersoff, Phys. Rev. Lett. **84**, 4393 (2000).].

The interface between silicon oxide and silicon plays a crucial role in modern semiconductor technology [1,2]. Because of the advancing miniaturization of semiconductor devices the atomic structure at the interface becomes increasingly important. Experimental access to the atomic structure at the interface is limited since the interface is buried below the isolating surface and due to the loss of long range order of the amorphous silicon oxide. The thermally grown SiO_2/Si(100) interface has been studied extensively during the last years leading to various different proposed interface structure models [1,2]. Presently, some investigations suggest a chemically graded interface with the suboxides distributed over a range of 20 Å [3] and others propose an interface consisting of a single layer of Si^{2+} atoms [4]. Some theoretical studies involved guessing candidate structures [5] for the interface, whereas other works attempted to obtain an unbiased structure using unconstrained molecular dynamics [6] and Monte Carlo methods [3,4,7]. A frequently used experimental technique to investigate the SiO_2/Si interface structure is high-resolution core-level photoemission spectroscopy. Si$2p$ photoemission spectra show chemically shifted components (Si^0, Si^{1+}, Si^{2+}, Si^{3+}, Si^{4+}) [8] and allow to get individual information for Si atoms in different oxidation states (cf. Figure 1). The photoemission intensity as function of angle and/or kinetic energy depends on the local environment of the emitting atom [9,10]. This dependence is caused by final-state diffraction effects of the photoelectron wave. Photoelectron diffraction is a well established technique for the determination of surface or interface structures [9,11]. Structural information is obtained by comparison of the experimental data with simulation calculations. An advantage of photoelectron diffraction compared to many other surface sensitive analytic methods is the high sensitivity to the local arrangement of nearest neighbor atoms within the escape depth of the electrons. In a previous investigation angle-scanned photoelectron diffraction was successfully applied to analyze the structure of the Si suboxides at the SiO_2/Si(111) interface [12]. The

obtained results are in excellent agreement with the results proposed by the simple statistical cross-linking model [13].

In this Letter, we report on an angle-scanned photoelectron diffraction investigation of the SiO_2/Si(100) interface. This technique provides for the first time a direct experimental access to the individual atomic structures of Si atoms in various oxidation states at this technically important interface. We present data showing full 2π angle-scanned diffraction patterns of various oxidation states and compare the experimental with the simulated diffraction patterns. A subsequently performed R-factor analysis allows to determine structural parameters like bond angles and bond lengths.

The experiment was performed in a μ-metal UHV chamber equipped with a hemispherical electron analyzer (150 mm electron path radius). A clean Si sample was
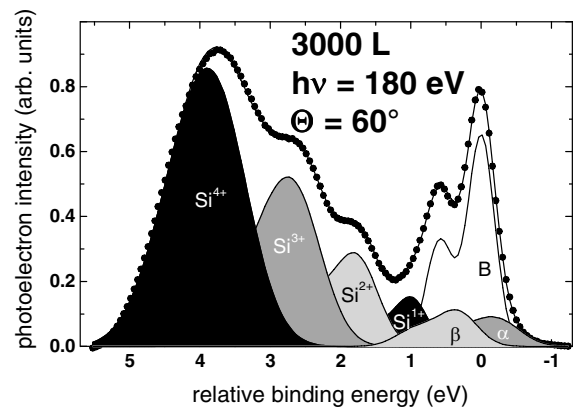

FIG. 1. Si$2p$ core-level spectrum recorded with a photon energy of $h\nu = 180$ eV for a silicon oxide film (3000 langmuir, $T_{sample} = 650\,°C$) on Si(100) at a polar-angle of $\Theta = 60°$. The binding energy is related to the Si$2p$ bulk position. The data points are denoted by symbols; the result of least squares fitting on this spectra is shown as a full line. Also, the decomposition into the bulk component and its six chemically shifted components due to the oxidation are shown.

obtained by heating the sample to 1050 °C for two min followed by a slow temperature decrease to room temperature. Thin SiO_2 films were grown *in situ* by thermal oxidation, the oxygen pressure was kept at 5×10^{-6} mbar for ten minutes equivalent to 3000 langmuir, while the crystal was held at a temperature of 650 °C. The electron energy resolution was about 50 meV and the photon energy resolution was set to 90 meV at a photon energy of 180 eV. At a fixed polar angle, photoemission spectra were recorded at the BESSY II U41-PGM beamline over 360° azimuth range with an increment of $\Delta\Phi = 2°$. Subsequently, a new polar-angle was set with an increment of $\Delta\Theta = 2°$ and a new azimuth scan was recorded. This was repeated until the full polar and azimuth range was covered ($0° < \Theta < 84°, 0° < \Phi < 360°$).

The experimental patterns were compared with results from multiple-scattering calculations for model clusters. Subsequently, an R-factor analysis for various structure parameters was included. The multiple-scattering calculations were performed using the MSPHD program package [14]. This software was developed to simulate Surface-Core-Level-Shift Photoelectron Diffraction (SCLS-PD) data and it was successfully applied to experimental data for a Si(100)-(2×1) surface by Gunnella *et al.* [15]. The analysis of the experimental data was performed by finding the minimum of the R-factor within an automatized procedure. This procedure was taken from tensor-LEED investigations [16], and here it was adopted to photoelectron diffraction pattern analysis. Figure 1 shows a typical photoemission spectrum of the oxidized Si surface after the secondary background has been subtracted. The line shape consists of seven resolved components, which correspond to the electron signals of Si^0 ($B + \alpha + \beta$), Si^{1+}, Si^{2+}, Si^{3+}, and Si^{4+}. The Si^0 signal was composed of the bulk signal (B) and two extra components (α, β). These components are assumed to be due to strained interfacial Si without any Si-O bonds [17]. Further details of the fitting procedure are given in Ref. [18].

Figure 2 displays the experimental (left column) and the simulated (right column) diffraction patterns of the Si atoms in various oxidation states. The patterns display the anisotropy function $\chi(\Theta, \Phi) = [I(\Theta, \Phi) - I_0(\Theta)]/I_0(\Theta)$ in a strictly linear gray scale, where $I(\Theta, \Phi)$ denotes the photoelectron intensity obtained by the above-mentioned fitting procedure and $I_0(\Theta)$ denotes the mean intensity for a given polar angle. The diffraction pattern of the bulk signal (Si^B) displays an intensity variation similar to the Si^B pattern of the clean Si(100)-(2×1) or the hydrogen terminated Si(100):H-2×1 surface [19]. The diffraction pattern of the suboxide Si^{2+} signal consists of elongated maxima at $\Phi = 45°, 135°, 225°, 315°$ azimuth direction. The Si^{4+} signal displays a completely different diffraction pattern. The main maxima are observed in $\Phi = 0°, 90°, 180°, 270°$ azimuth direction. The different diffraction patterns reflect the individual local environment of each oxidation state.
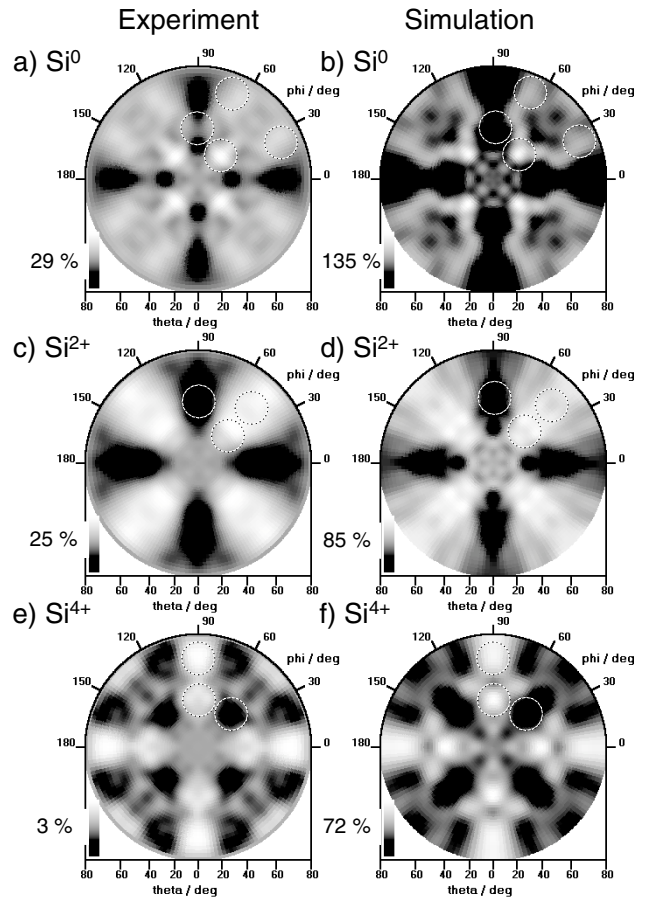

FIG. 2. Experimental (left column) and simulated (right column) Si$2p$ diffraction patterns of silicon in different oxidation states (Si^0, Si^{2+}, Si^{4+}) obtained for a photon energy of $h\nu = 180$ eV. In the simulation the structure displayed in Fig. 3 was used.

In order to compare experimental diffraction patterns with simulated patterns, it is necessary to have a first idea of the interface structure. A structural element, which was consistently proposed by various structure models of the SiO_2/Si interface [3–5,7], is a silicon crystal terminating Si-O-Si brigde bond. Tersoff *et al.* [4] suggested such a SiO_2/Si(100) interface obtained by Monte Carlo simulations. Their "canonical" interface structure connects the ideally bridge-bonded Si to the amorphous SiO_2 through a single layer of Si^{2+}. The bridge bond eliminates half of the bonds from the Si side, correcting the mismatch between the bond densities in the two different materials. Several experiments [8,17,18,20] and further investigations of Tersoff *et al.* [7] reveal that the interface structure can not be perfectly ordered. For instance, recent ion scattering investigations [20] of the SiO_2/Si(100) interface found silicon displacements larger than 0.09 Å propagating for three layers into the Si substrate, ruling out a transition with regularly ordered O bridges. Furthermore, Oh *et al.* [17] reported on an analysis of the suboxide Si$2p$ photoemission polar-angle dependence. The result from these observations is a

graded interface consisting of three layers with a significant amount of atoms in a Si^{1+} and a Si^{3+} oxidation state. It was shown [18] that the photoemission polar-angle dependence of all Si suboxides at the $SiO_2/Si(100)$ interface can be explained within a simple statistical model. The fit of the model curves to the experimental data reveals a decrease of the Si density in the second interface layer to half of the Si-bulk density. This sharp transition of the silicon density can be explained by the above-mentioned Si-O-Si bridge bonds. Within the statistical three layer interface model [18] a nearly perfect interface is formed between the first and the second layer due to the strong influence of the silicon crystal structure. The model predicts for the Si atoms in the first interface layer that $\frac{4}{9}$th, $\frac{4}{9}$th, and $\frac{1}{9}$th of the atoms are in the Si^{1+}, Si^{2+}, and Si^0 oxidation states, respectively. The Si^{3+} and Si^{4+} atoms are predicted to be in the second and third interface layer.

Our calculations for Si^{2+} and Si^{4+} atoms were started with the canonical interface structure suggested by Tersoff *et al.* [4] (cf. configuration on the left of Fig. 3). Only scatter atoms within a radius of 6 Å around the emitter atom were considered because of the lack of a long range order at the interface. In addition, silicon displacements propagating into the Si substrate are allowed. Figure 3 displays the structure model and the structural parameters which are optimized during the R-factor analysis. Also, possible Si^{1+} and Si^{3+} atom sites are shown. Assuming the SiO_2 layer completely amorphous, the Si^{4+} diffraction pattern is mainly determined by the interfacial Si^{4+}. The local environment of Si^{2+} atoms in the first interface layer is very different (cf. Fig. 3). This is also indicated by the diffraction patterns of the two suboxide species (cf. Fig. 2). Therefore, an R-factor analysis was performed optimizing both the Si^{4+} and Si^{2+} diffraction patterns, simultaneously. A random scattering in the amorphous SiO_2 film leads to a

damped electron intensity and to a broadening of the diffraction maxima [21]. Therefore, the maximum anisotropy of the diffraction pattern is reduced while the basic intensity variation of the pattern is preserved. Another reason for the rather low anisotropy of the Si^{4+} pattern ($\chi = 3\%$, Fig. 2) is the small number of interfacial Si^{4+} emitter atoms in the second layer compared to the total number of Si^{4+} atoms.

Analysis of experimental data was performed within an R-factor analysis for the structure parameters. The R factor is defined as a sum over the range of data points:

$$R = \frac{\Sigma_i(\chi_{th} - \chi_{exp})^2}{\Sigma_i\chi_{th}^2 + \chi_{exp}^2} \quad (1)$$

where χ_{exp} and χ_{th} denote the normalized anisotropy functions of experiment and simulation, respectively. The minimum R-factor $R = 0.14$ is obtained for $d = 1.82 \pm 0.02$ Å, $\alpha = 20° \pm 1°$, $x = 0.18 \pm 0.02$ Å, $z_1 = +0.01 \pm 0.02$ Å, $z_2 = +0.5 \pm 0.02$ Å, and $z_3 = -0.27 \pm 0.02$ Å by the above-mentioned search procedure. The R-factor depends mainly on the parameters d and α, plotted in Fig. 4. All other parameters are kept constant at the R-factor minimum values. The main minimum of the R factor is located at $d = 1.82$ Å and $\alpha = 20°$, and two further minima are shown at $d = 1.51$ Å, $\alpha = 23°$ and $d = 1.57$ Å, $\alpha = 19°$. The main minimum with $R = 0.14$ is smaller than the two weaker minima with $R = 0.2$. It was verified by a Levenberg-Marquadt [22] minimum search routine that the minimum at $d = 1.82$ Å and $\alpha = 20°$ is the global minimum. Within this procedure, the parameters of the three minima and the parameters of some randomly chosen points were used as starting points and all parameters were varied. No further minima with an R-factor less than 0.19 were found.

The suboxide signals of Si^{1+}, Si^{2+}, and Si^{3+} show similar diffraction patterns indicating a similar vicinity
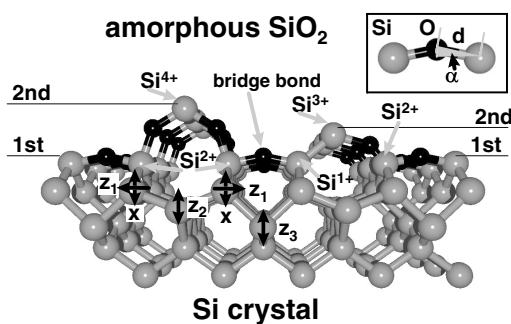

FIG. 3. Side view of the interface structure model used to calculate the diffraction patterns: The two possible transitions between the first and the second interface layer are displayed. In the first case only Si^{2+} is involved (left side) whereas in the second case also Si^{1+} is present (right side). Further, the parameters (d, α, x, z_i) are displayed which are varied during the R-factor analysis for the Si^{4+} and the Si^{2+} diffraction patterns (Si gray spheres; O black spheres).

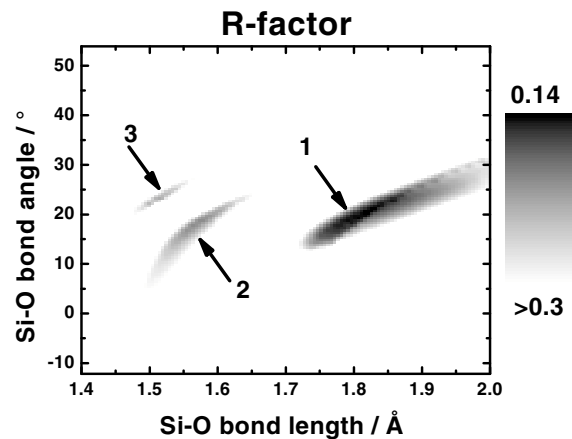

FIG. 4. R factor as a function of the Si-O bond length d and the Si-O bond-angle α. The local minima are located at $d = 1.82$ Å, $\alpha = 20°$ (1); $d = 1.57$ Å, $\alpha = 19°$ (2); and $d = 1.51$ Å, $\alpha = 23°$ (3), respectively.

[18]. Therefore, we used the structural parameters obtained by the R-factor analysis for $Si^{2+} + Si^{4+}$ to form a Si^{1+} cluster. In addition, we assume the bond length between the Si^{1+}-atom and the Si atom above is equivalent to the bulk bond length of 2.35 Å. As in the case of the Si^{2+} patterns, there is good agreement between the experimental and the simulated data.

The minimum R factor was found for a silicon-oxygen distance of $d = 1.82$ Å, which is 12–17 % larger than the values obtained for the fourfold-coordinated crystalline polymorphs of silica (quartz, cristobalite, tridymite, and coesite, d =1.55– 1.62 Å [23]). Similar bond lengths were found for an ultrahigh pressure polymorph of silica called stishovite with $d = 1.809$ Å [23]. Stishovite is a more densely packed SiO_2 structure, with silicon in octahedral (sixfold) coordination with oxygen, which is inconsistent with our fourfold-coordinated model. Further, the bond-angle $\alpha = 20°$ is larger than the angles found for the fourfold-coordinated polymorphs (≤ 18.15 [23]).

A comparison of the experimental diffraction patterns with the diffraction patterns obtained for the parameter set of the minimum R factor shows small deviations (cf. Figure 2). All main features of the experimental data are reproduced by the simulation. Generally, the experimental diffraction patterns display a lower anisotropy than the simulated patterns. A better agreement between experiment and simulation may be achieved by taking into account the elastic scattering within the amorphous SiO_2 film. Further, within the transition from the perfect Si-bulk structure to the amorphous SiO_2 film, several slightly different interface structures are possible. The experimental observation of Si^{1+} and Si^{3+} signals (cf. Fig. 1) indicates their presence within the interface. Thus, we can find defect structures containing the Si^{1+} and Si^{3+} suboxides in the vicinity of a perfect bridge-bond structure composed of Si^{2+} suboxides. The defect structures induce site displacements and bond-angle variations from the perfect bridge-bond structure, and therefore the experimental diffraction pattern deviates from the diffraction pattern of the model structure.

In summary, we investigated the local environment of Si at the interface between a thermally grown SiO_2 film and a Si(100) crystal. We utilize the chemically shifted Si2p core-level photoelectrons as a local probe at the interface. The Si^{x+} photoelectron diffraction patterns contain information about the structural environment of Si atoms in the various oxidation states. The comparison of the diffraction patterns with multiple-scattering calculations including an R-factor analysis supports the Si-O-Si bridge-bond interface model. The excellent agreement between the experimental and the simulated data for a small cluster size (6 Å radius) shows no evidence for a superlattice at the interface. The obtained values for the Si-O bond length and the bond-angle deviate from previously found values for the fourfold-coordinated crystalline polymorphs of silica.

[1] T. Hattori, Crit. Rev. Solid State Mater. Sci. **20**, 339 (1995), and references therein.
[2] L. C. Feldman, in *Fundamental Aspects of Silicon Oxidation*, edited by Y. J. Chabal (Springer-Verlag, Berlin, 2001).
[3] K.-O. Ng and D. Vanderbilt, Phys. Rev. B **59**, 10132 (1999).
[4] Yuhai Tu and J. Tersoff, Phys. Rev. Lett. **84**, 4393 (2000).
[5] A. Pasquarello, M. S. Hybertsen, and R. Car, Appl. Phys. Lett. **68**, 625 (1996).
[6] A. Pasquarello, M.S. Hybertsen, and R. Car, Nature (London) **396**, 58 (1998).
[7] Yuhai Tu and J. Tersoff, Phys. Rev. Lett. **89**, 086102 (2002).
[8] F. J. Himpsel, F. R. McFeely, A. Taleb-Ibrahimi, J. A. Yarmoff, and G. Hollinger, Phys. Rev. B **38**, 6084 (1988).
[9] C. S. Fadley, Surf. Sci. Rep. **19**, 231 (1993).
[10] D. P. Woodruff and A. M. Bradshaw, Rep. Prog. Phys. **57**, 1029 (1994).
[11] C. Westphal, Surf. Sci. Rep. **50**, 1 (2003).
[12] S. Dreiner, M. Schürmann, C. Westphal, and H. Zacharias, Phys. Rev. Lett. **86**, 4068 (2001).
[13] D.-A. Luh, T. Miller, and T.-C. Chiang, Phys. Rev. Lett. **79**, 3014 (1997).
[14] R. Gunnella, F. Solal, D. Sébilleau, and C. R. Natoli, Comput. Phys. Commun. **132**, 251 (2000).
[15] R. Gunnella, E. L. Bullock, L. Patthey, C. R. Natoli, T. Abukawa, S. Kono, L. S. Johansson, Phys. Rev. B **57**, 14739 (1998).
[16] M. Kottcke and K. Heinz, Surf. Sci. **376**, 352 (1997).
[17] J. H. Oh, H. W. Yeom, Y. Hagimoto, K. Ono, M. Oshima, N. Hirashita, M. Nywa, A. Toriumi, A. Kakizaki, Phys. Rev. B **63**, 205310 (2001).
[18] S. Dreiner, M. Schürmann, and C. Westphal, J. Electron Spectrosc. Relat. Phenom. **137-140**, 79 (2004).
[19] S. Dreiner, C. Westphal, M. Schürmann, and H. Zacharias, Thin Solid Films **428**, 123 (2003).
[20] A. Bongiorno, A. Pasquarello, M. S. Hybertsen, and L. C. Feldman, Phys. Rev. Lett. **90**, 186101 (2003).
[21] T. Hattori, K. Hirose, H. Nohira, K. Takahashi, and T. Yagi, Appl. Surf. Sci. **144-145**, 297 (1999).
[22] W. H. Press, S. A Teukolsky, W. T. Vetterling, and B. P. Flannery, *Numerical Recipes in C* (Cambridge University Press, Cambridge, England, 1992).
[23] Th. Demuth, Y. Jeanvoine, and J. G. Ángyán, J. Phys. Condens. Matter **11**, 3833 (1999).